ACS APPLIED MATERIALS & INTERFACES

Research Article

www.acsami.org

Atomistic Origins of High Capacity and High Structural Stability of Polymer-Derived SiOC Anode Materials

Hong Sun and Kejie Zhao*

School of Mechanical Engineering, Purdue University, West Lafayette, Indiana 47907, United States

ABSTRACT: Capacity and structural stability are often mutually exclusive properties of electrodes in Li-ion batteries (LIBs): a gain in capacity is usually accompanied by the undesired large volumetric change of the host material upon lithiation. Polymer-derived ceramics, such as silicon oxycarbide (SiOC) of hybrid Si−O−C bonds, show an exceptional combination of high capacity and superior structural stability. We investigate the atomistic origins of the unique chemo-mechanical performance of carbon-rich SiOC using the first-principles theoretical approach. The atomic model of SiOC is composed of continuous Si−O−C units caged by a graphene-like cellular network and percolated nanovoids. The segregated sp^2 carbon network serves as the backbone to maintain the structural stability of the lattice. Li insertion is first absorbed at the nanovoid sites, and then it is accommodated by the SiOC tetrahedral units, excess C atoms, and topological defects at the edge of or within the segregated carbon network. SiOC expands up to 22% in volumetric strain at the fully lithiated capacity of 1230 mA h/g. We examine in great detail the evolution of the microscopic features of the SiOC molecule in the course of Li reactions. The first-principles modeling provides a fundamental understanding of the physicochemical properties of Si-based glass ceramics for their application in LIBs.

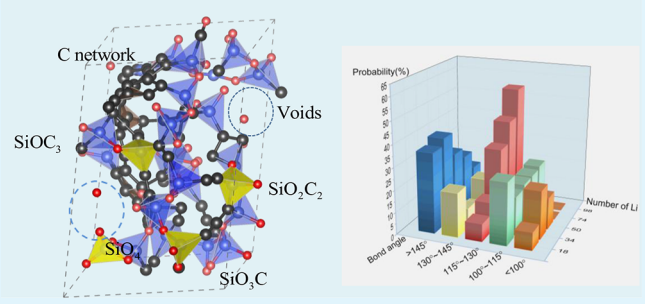

KEYWORDS: *SiOC, high capacity, structural stability, first principles, lithiation*

INTRODUCTION

Li-ion batteries (LIBs) are the current choice for powering portable electronics and electric vehicles. The capacity of a LIB is theoretically limited by the electrode materials. The most commonly used anode in LIBs is graphite because of its stable cycle ability, high Coulombic efficiency, and structural stability.[1] However, the key drawback of low reversible capacity limits its application in high-energy-density batteries.[2] A variety of Si-based composites are currently being explored to replace the conventional graphite anodes. One Si atom can alloy with 3.75 Li atoms, whereas six C atoms can only host 1 Li atom, which results in the specific capacity of Si that is 10 times higher than that of graphite. However, the limiting factor with Si is the drastic volumetric change (up to 400%) associated with Li insertion and extraction, which causes tremendous mechanical issues in the practical implementation of Si anodes.[3,4] In fact, capacity and structural stability are mutually exclusive properties of most electrodes: a gain in capacity is often associated with the large volumetric change and sacrifice of the structural stability of the host material upon lithiation. To mitigate the mechanical failure of high-capacity electrodes, many novel hybrid chemistries and architectures have been proposed.[5−7] Nevertheless, a composite made of separate phases such as Si and C does not resolve the issue of intrinsic volumetric expansion and subsequent degradation of Si—the continuous shedding of Si upon lithiation cycles remains a major challenge in spite of many clever designs of composite structures.

Therefore, a natural question is that, is there a compound, likely with hybrid Si−C atomic bonds, which can combine the strength of C (superior structural stability in lithiation cycles) and Si (high capacity) to overcome the trade-off between capacity and mechanical stability? Polymer-derived ceramics [such as silicon oxycarbide (SiOC)] present a viable solution.[8] Si-based glass ceramics react with Li at a potential ranging from 0 to 2.5 V (vs Li/Li^+) and deliver a charge capacity of ∼600 mA h/g with a robust mechanical stability over a thousand cycles.[9] Moreover, these ceramics can be conveniently molded into any desired shape, size, structure, or morphology as demanded by the application, and the final properties of the ceramics can be tailored by the type of the polymeric precursor and processing conditions.[10−13]

The electrochemical capacity of SiOC is attributed to its amorphous nanodomain structure, which is composed of a segregated C network, SiO_xC_{4-x} tetrahedral units, and nanovoids.[9] This paper aims to explore the thermodynamics of Li reactions and microstructural evolutions in SiOC and to investigate the atomistic origins of the high capacity and high structural stability of the Si-based glass ceramic during Li insertion. We adopt a carbon-rich $Si_{28}O_{42}C_{68}$ model to capture the salient features of Si−O−C composites: continuous SiO_xC_{4-x} tetrahedral units are caged by a graphene-like sp^2 C

Received: July 24, 2017
Accepted: September 20, 2017
Published: September 20, 2017

DOI: 10.1021/acsami.7b10906
ACS Appl. Mater. Interfaces 2017, 9, 35001−35009

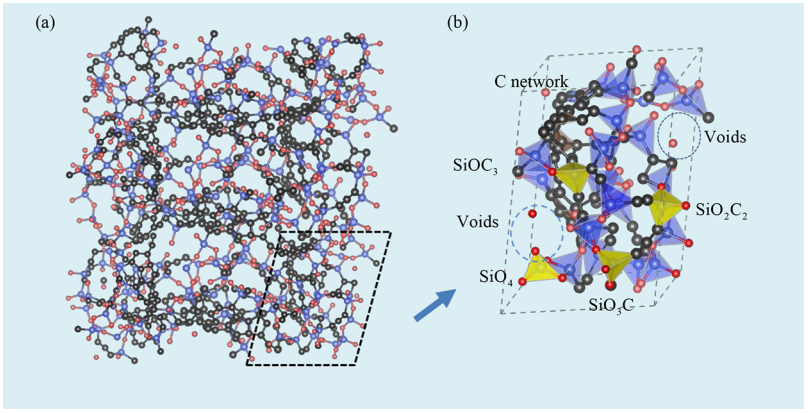

Figure 1. Atomic model of silicon oxycarbide (SiOC) consisting of the C phase, SiO_xC_{4-x} units, and nanovoids. (a) Overview of the supercell with an applied periodic boundary condition. (b) Unit cell shows a series of vertex-sharing tetrahedra including SiO_4, SiO_3C, SiO_2C_2, and $SiOC_3$. The gray atoms represent the segregated C phase which forms the backbone of the network. Excess C atoms are randomly distributed, and topological defects of five and seven C−C rings exist. The blue dotted circles mark the nanovoids percolated in the lattice which contribute to the low density of the SiOC molecule.

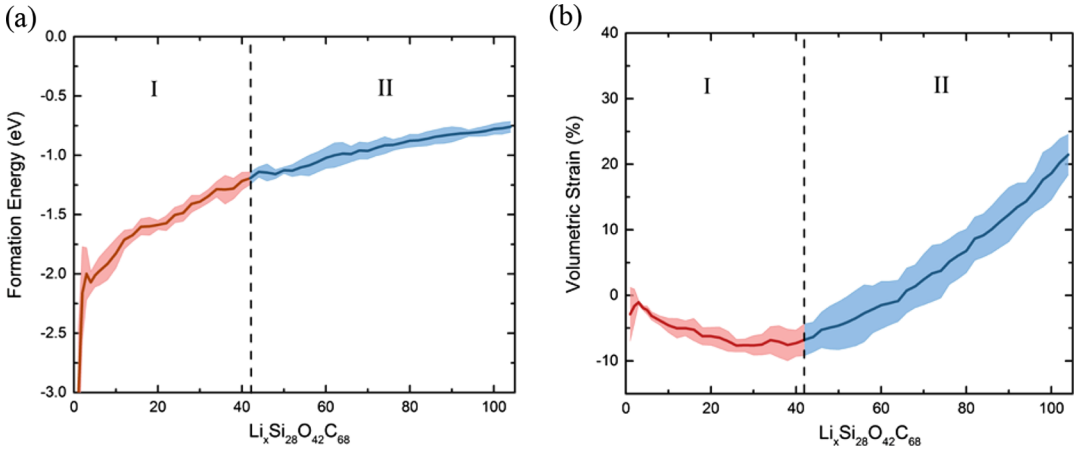

Figure 2. Two-step lithiation of SiOC shown in the (a) formation energy per Li in Li_xSiOC and (b) volumetric strain as a function of Li concentration. The solid lines represent the average values of the formation energy per Li or the volumetric strain from the five configurations at a given Li concentration, and the error bars represent the standard deviation. The red lines indicate Li intercalation at the nanovoids. The formation energy per Li in this stage shows a large variation at a given Li concentration because of the large difference in the local bonding environment. The lattice volume decreases due to the structural relaxation mediated by Li insertion. The blue lines delineate Li reactions with the SiOC tetrahedral units and the C phase. Both the formation energy and the volumetric strain reach a steady slope as Li is inserted in stage II.

cellular network, whereas nanovoids are percolated in the lattice. The nanodomain size in the model is well-consistent with the experimental result.[14] The high capacity originates from Li absorption at the percolated nanovoid sites, followed by Li reactions with the C phase and Si−O−C units. The segregated sp^2 C interface remains nearly inactive in the lithiation process and serves as the backbone to maintain the structural stability of the host material. SiOC expands up to 22% in volumetric strain after complete lithiation, which is several times smaller than the typical conversion- or insertion-type anode materials.[15] We perform a detailed statistical analysis on the microstructural features, including the evolution of the local bonding environment, tetrahedral units, geometry perturbation and relaxation, and electron transfer, to provide a complete understanding of the electrochemomechanical behavior of the SiOC anode material.

MODEL GENERATION

A reliable atomic structure of the glass ceramic is the key for small-scale quantum modeling. We generate the Si−O−C continuous network by randomly replacing O atoms in SiO_4 tetrahedra by C. Different types of Si−O−C tetrahedral units including SiO_4, SiO_3C, SiO_2C_2, and $SiOC_3$ are distributed in the network. The C-doped silica domain is caged by a graphene-like cellular network. The segregated C phase and the interface between the graphene-like C network and the Si−C−O units are generated by exploring over 180 possible local configurations using evolutionary algorithm implemented in the USPEX program.[16] The optimized cluster model containing a C network and SiO_xC_{4-x} units is input as the seed structure. The successive 180 structures are developed by 10 evolutional generations, and each generation is produced by the combined variation method of heredity, random space group specificity, soft mutation, and lattice mutation. The most favorable configuration of the least enthalpy is taken as the best structure. The whole amorphous cell is subject to annealing by ab initio molecular dynamics. NVT ensemble is maintained by a Nosé thermostat. Temperature is gradually increased from 300 to 1200 K and is maintained at a constant temperature of 1200 K for 2 ps. Then, the structure is slowly quenched from 1200 to 300 K with a quenching rate of 112 K/ps and is energetically relaxed at 0 K. After the annealing and quenching process, the amorphous cell has a nanodomain size of ∼1.5 nm and a mass density of 1.8 g/cm^3 which are in

DOI: 10.1021/acsami.7b10906
ACS Appl. Mater. Interfaces 2017, 9, 35001−35009

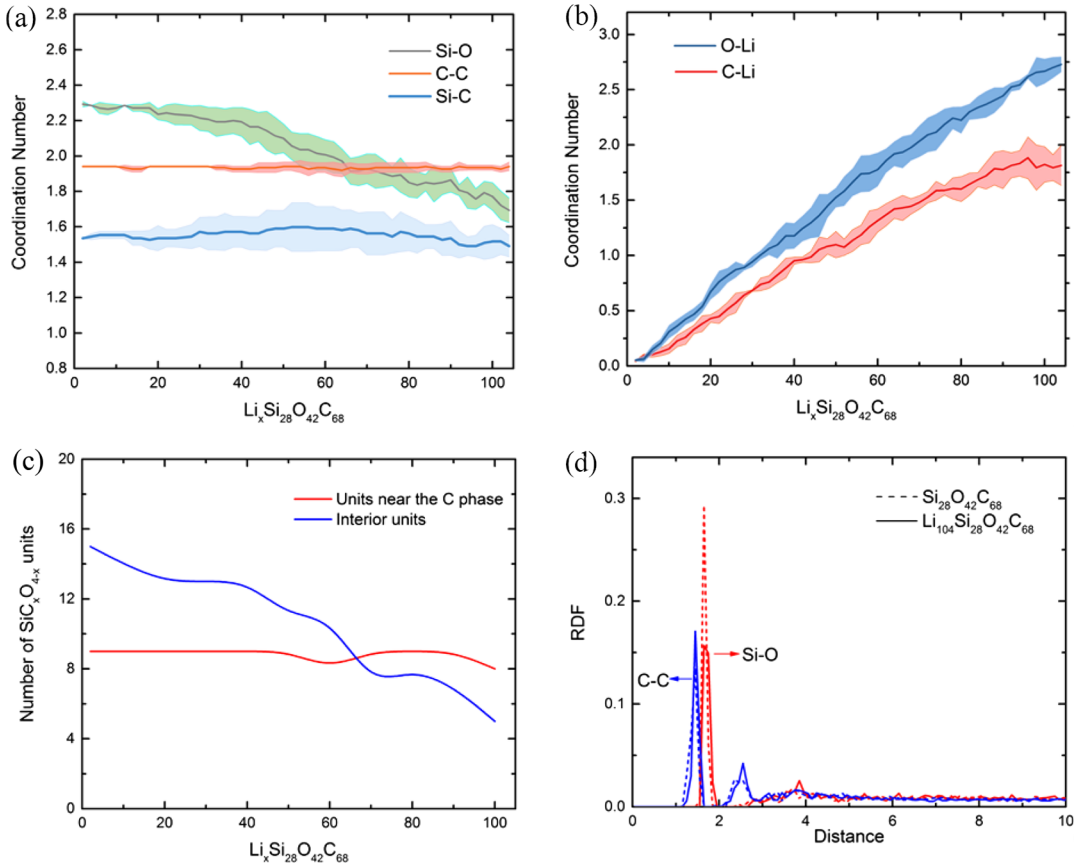

Figure 3. The structural feature of lithiated SiOC represented by the (a) coordination number of Si−O, C−C, and Si−C; (b) coordination number of O−Li and C−Li; (c) number of SiO_xC_{4-x} tetrahedral units; and (d) RDF of Si−O and C−C before and after lithiation. The coordination number in (a) corroborates the two-step lithiation that little change of chemical bonding is involved when Li composition is below $Li_{42}Si_{28}O_{42}C_{68}$, while further lithiation is associated with the breaking of Si−O bonds. The increasing coordination number of O−Li and C−Li in (b) indicates that Li atoms are attracted by the O and C atoms. The statistics of the SiO_xC_{4-x} tetrahedral units in (c) shows that the number of the interior units caged in the network steadily decreases, whereas the units residing in the vicinity of the segregated C phase remain nearly unperturbed upon lithiation. The RDF of Si−O and C−C in (d) again shows the local stable bonding of C−C and severe breaking of Si−O upon Li insertion.

good agreement with the experimental measurements.[14,17] The generated supercell contains the salient features of SiOC including the continuous Si−O−C network, segregated C interface, and nanovoids. We have ignored the presence of H in SiOC which is determined to be around 5% in atomic percentage by prior experiments.[9] The presence of H may affect the tendency of carbon clustering in the initial SiOC structure;[18] however, such an effect may become less significant as lithiation proceeds because the large fraction of Li plays a dominant role in the chemistry of SiOC.

COMPUTATIONAL METHODS

We employ first-principles modeling within the framework of density functional theory (DFT) to investigate the microscopic mechanism of lithiation in SiOC. Projector-augmented-wave potentials in a Vienna Ab initio Simulation Package are used to mimic the ionic cores, and the generalized gradient approximation in the Perdew−Burke−Ernzerhof (PBE) flavor is employed for the exchange and correlation functional.[19,20] The atomic structures and system energy are calculated with an energy cutoff of 400 eV. For Brillouin zone sampling, a 2 × 2 × 2 mesh of k points in the Monkhorst−Pack scheme is sufficient in the energetic relaxation of Li_xSiOC. The energy optimization is considered complete when the magnitude of the force on each atom is smaller than 0.04 eV·Å^{-1}.

Energetic calculations are employed to examine the thermodynamics of Li insertion. We incrementally increase Li concentration to model the lithiation process. We consider five possible configurations of Li_xSiOC at a given Li concentration with different Li distributions in each, to eliminate the large variations inherent to the small model size. At each Li concentration, we perform the Delaunay triangulation analysis to identify the possible favorite sites for Li insertion.[21,22] Formation energy per Li at various Li concentrations is calculated to represent the thermodynamic driving force of Li insertion into SiOC. We take the energy of SiOC and the energy of a Li atom in its bulk form (E_{Li}) as the reference energies, with $E_{nLi-SiOC}$ being the total energy of the system containing n number of Li atoms in the cell. The formation energy per Li atom $E_f(n)$ is calculated as $E_f(n) = [E_{nLi-SiOC} - E_{SiOC} - nE_{Li}]/n$.

The geometries of isolated Si−C−C−Si clusters before and after lithiation are studied by the molecular orbital (MO) analyses. The single-point energy calculation of two configurations is performed to obtain the wave function of the particular arrangement of nuclei using the Gaussian 09 package.[23] The hybrid functional B3LYP with the 3-21+G* basis set is employed for the DFT calculations. The selected MOs of the centered C atoms are plotted by Multiwfn software.[24]

RESULTS AND DISCUSSION

The polymer-derived SiOC has a heterogeneous molecular structure of amorphous nature, which contains silica domains, Si−O−C hybrid bonds, a graphene-like carbon network, and nanovoids.[9] Figure 1a gives an overview of the carbon-rich SiOC supercell model with an applied periodic boundary condition. Figure 1b shows the unit cell containing 28 Si atoms, 42 O atoms, and 68 C atoms. The lattice parameters of the amorphous unit cell are a = 1.4 nm, b = 1.1 nm, and c = 1.5 nm, corresponding to

DOI: 10.1021/acsami.7b10906
ACS Appl. Mater. Interfaces 2017, 9, 35001−35009

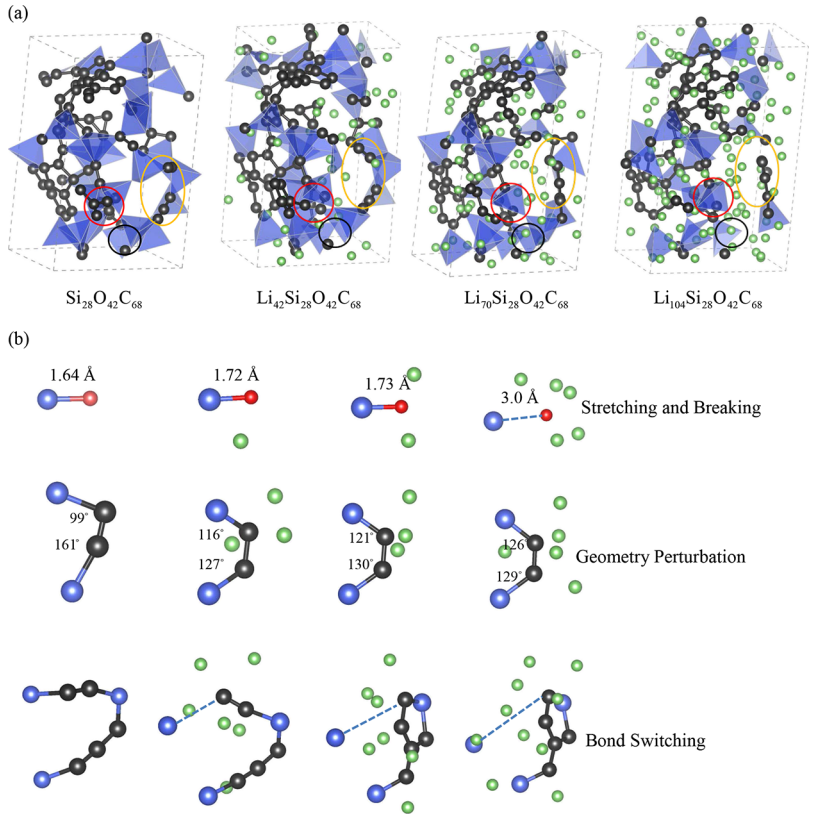

Figure 4. (a) Evolution of atomic configurations of SiOC during lithiation. The backbone of segregated C phase stabilizes the structure. The cell volume changes up to 22% after full lithiation. (b) Local structural rearrangement in the atomic configurations in (a) includes stretching and breaking of Si−O bonds, geometry perturbation of Si−C−C−Si clusters, and bond switching in C rings. The purple, red, gray, and green spheres represent the Si, O, C, and Li atoms, respectively.

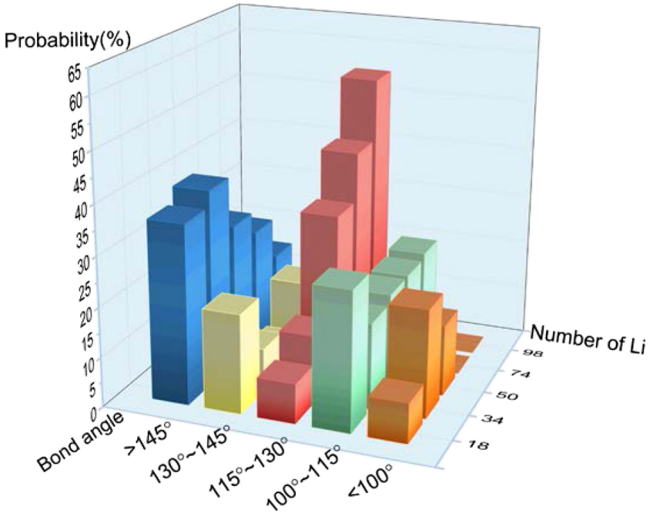

Figure 5. Bond angle distribution of C−C−C, Si−C−C, and Si−C−Si clusters in five representative Li_xSiOC compositions. The salient features are that the probability of bond angles larger than 145° steadily decreases, whereas the distribution of bond angles between 115° and 130° increases significantly upon lithiation. This demonstrates the geometry optimization of C atoms toward the sp^2 type coordinated by Li insertion.

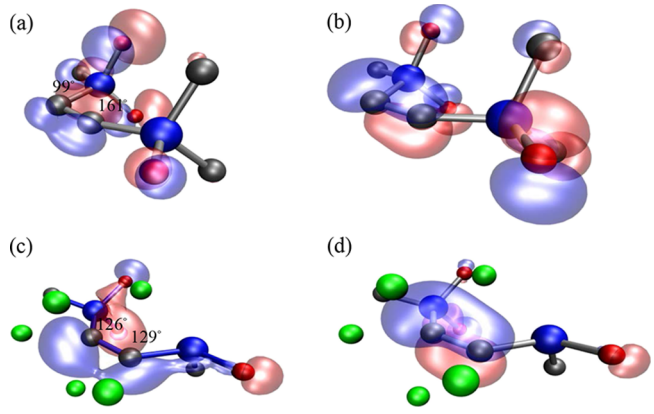

Figure 6. Evolution of two MOs contributed by two centered C atoms in a Si−C−C−Si cluster. (a) Before lithiation, the p_y orbitals of the two C atoms overlap to form one π-type MO, π_y. (b) Similarly, two p_z atomic orbitals overlap to form the π_z orbital. (c) After lithiation, the original π_y orbital is perturbed by the virtual orbital of the nearby Li atoms (not shown in the diagram) and is split into two atomic orbitals in different orientations, which promotes the formation of the hybrid sp^2 orbital. (d) In comparison, there is no obvious difference in π_z which remains perpendicular to the sp^2 hybrid planar orbital before and after lithiation.

the well-accepted nanodomain size of SiOC (1−5 nm) in the experimental measurement.[14] This size of the unit cell is consciously relatively small for the exploration of a large number of possible configurations of the glass ceramics with various Li concentrations. The choice of the model size affords our explorations at a reasonable computational cost without sacrificing the accuracy of the microscopic features of the heterogeneous structure. The gray atoms in Figure 1b represent the segregated C phase which forms the stable backbone of the molecule structure. In the graphene-like C regime, topological

DOI: 10.1021/acsami.7b10906
ACS Appl. Mater. Interfaces 2017, 9, 35001−35009

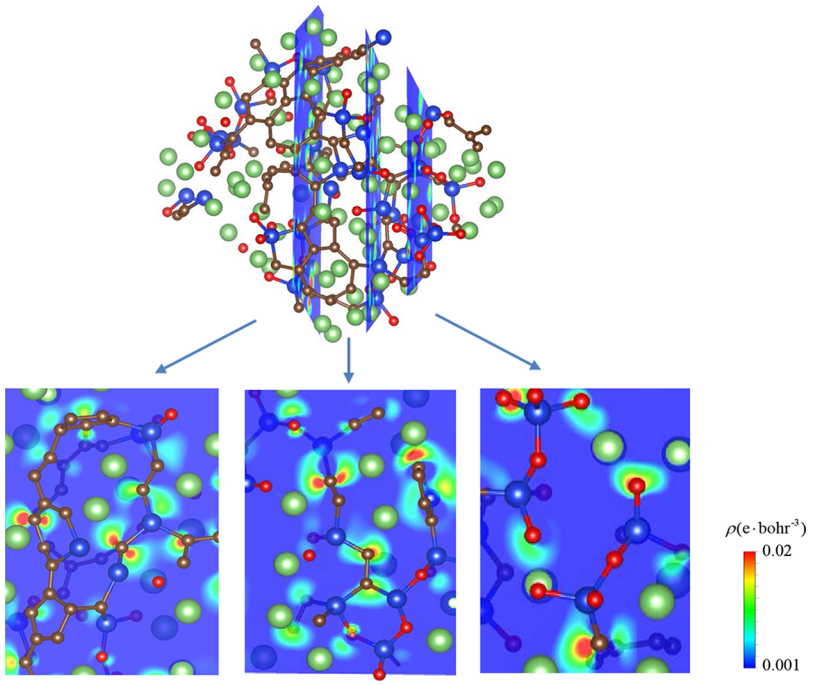

Figure 7. Map of charge-density difference in different regions of $Li_{66}Si_{28}O_{42}C_{68}$. From left to right, it shows the charge-density difference of the segregated C interface, the Si−O−C mixed regime, and the amorphous silica domain before and after Li insertion, respectively. In the graphene-like C phase, charge transfer takes place at the imperfection sites such as the five or seven C rings or the edge of C atoms. The saturated sp^2 C atoms remain inactive and serve as the stable backbone to maintain the structure. In the mixed Si−O−C regime, charge transfer mainly occurs around the O atoms and unsaturated C atoms. For the SiO_4 tetrahedral units in the silica domain, positive charge is accumulated around the O atoms.

defects such as five- or seven-membered C rings exist. The vertex-sharing tetrahedra represent the randomly distributed Si−O−C units. After annealing, the excess C atoms are distorted to form short C−C chains.[18] Many of the C atoms are unsaturated with dangling bonds. Different types of SiO_xC_{4-x} tetrahedral units including SiO_4, SiO_3C, SiO_2C_2, and $SiOC_3$ are included in the network,[25] which are highlighted in Figure 1b. The blue dotted circles mark the nanovoid regimes percolated in the unit cell, which contribute to the low density of the SiOC molecule (~1.8 g/cm^3).[17]

Figure 2a shows the formation energy per Li in lithiated SiOC. The solid line represents the average values from five different configurations for each Li composition, and the error bars (the height of the shaded area at a given Li concentration) represent the standard deviation. The negative formation energy indicates that the Li reaction is thermodynamically favorable. The lithiation process can be roughly divided into two stages: Li absorption at the nanovoids in stage I and Li alloying with SiOC units, excess C atoms, and the defect sites within the C network in stage II. The two-step lithiation is reflected in the variation of the slope of the formation energy with a transient composition of $Li_{42}Si_{28}O_{42}C_{68}$. The first stage is marked with a red line. The initial open structure provides a variety of spots and a large driving force for Li insertion. The formation energy per Li in a given composition shows a relatively large variation because of the different local bonding environment in the nanovoid regimes where Li gradually fills in. In the second stage (blue line) where Li composition is higher than $Li_{42}Si_{28}O_{42}C_{68}$, the nanovoids are nearly saturated. The thermodynamic driving force for Li insertion decreases. The variation of formation energy per Li in the five different configurations with the same Li concentration becomes small, which implies that the local chemical environments for Li reactions are roughly the same. Figure 2b plots the volumetric strain of SiOC as a function of Li concentration which again delineates the two-step lithiation. When Li concentration is below $Li_{42}Si_{28}O_{42}C_{68}$, the volume of SiOC decreases because of the structural relaxation mediated by Li. Li fills the nanovoids and tightens the structure through the electrostatic interaction with the surrounding anionic O atoms and unsaturated C atoms. This behavior is consistent with a previous study on $Li_{1/2}SiC_{1/4}O_{7/4}$[26] as well as the experimental observation of Li intercalation in microporous Si−O−C composite materials.[14] When the transient composition of $Li_{42}Si_{28}O_{42}C_{68}$ is passed, the volumetric strain increases linearly with a partial molar volume of Li, that is, Ω = 10.0 Å^3 which is close to the partial molar volume of Li in pure silica.[22] SiOC expands by 22% in the volumetric strain upon the full lithiation capacity of 1230 mA h/g. It is worth noting that the volumetric strain of SiOC is much smaller than that of conversion- or insertion-type high-capacity anodes which are typically on the order of magnitude of 100%.[15] The small volumetric change retains the mechanical stability of SiOC in the course of lithiation and grants the glass ceramic an exceptional combination of high capacity and high structural stability. The two-step lithiation is accompanied by a continuous structural rearrangement of SiOC which will be closely examined as follows.

To explore the structural evolution of SiOC upon lithiation, the statistics of the local bonding environment, including the coordination number, radial distribution function (RDF), and the number of SiOC tetrahedral units, are analyzed and plotted in Figure 3. Figure 3a shows the variation of the coordination number of Si−O, C−C, and Si−C in different Li_xSiOC compositions, respectively. The three solid lines represent the average values from five different configurations for each composition, and error bars represent the standard deviation. To have a physical measure of the atomic coordination, we define

DOI: 10.1021/acsami.7b10906
ACS Appl. Mater. Interfaces 2017, 9, 35001−35009

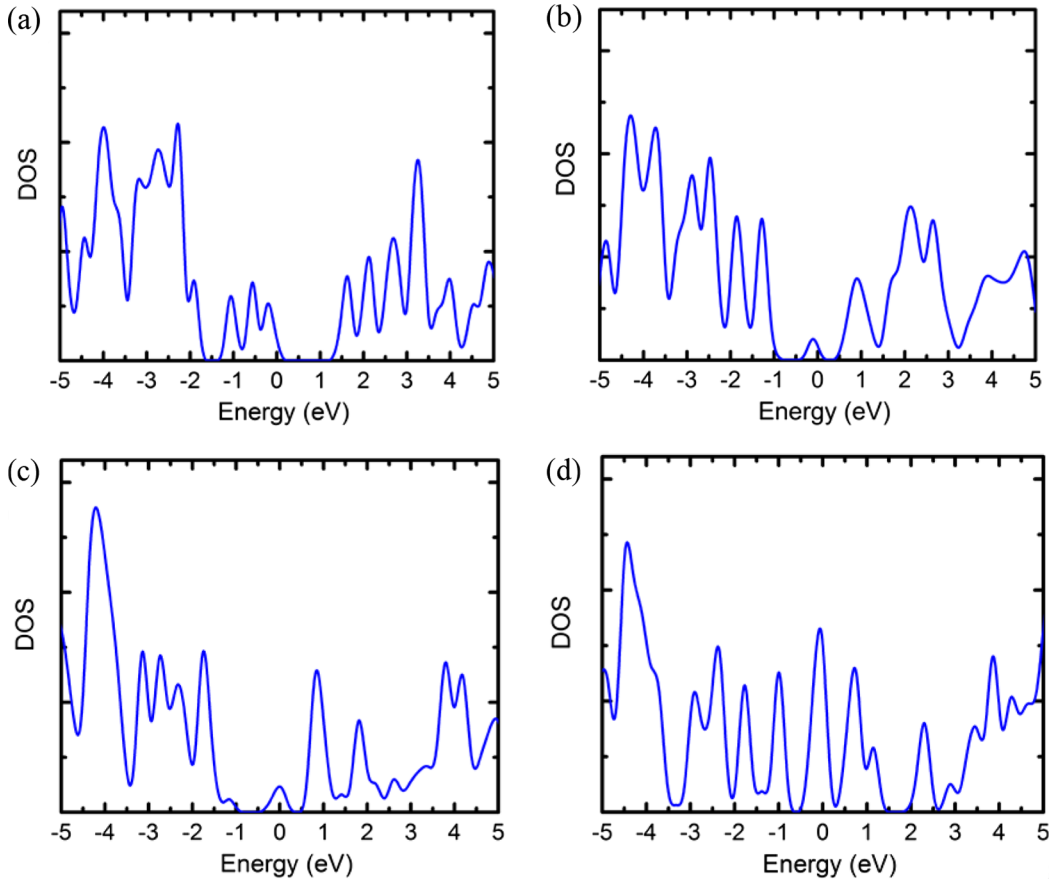

Figure 8. DOS of (a) pristine SiOC, (b) $Li_2Si_{28}O_{42}C_{68}$, (c) $Li_4Si_{28}O_{42}C_{68}$, and (d) $Li_6Si_{28}O_{42}C_{68}$, respectively. The DOS of pristine SiOC has an insulator character with a band gap of 1.3 eV. During initial lithiation, the electron transfer from Li to O and defective C atoms induces electron states near the Fermi level. The band gap is significantly reduced by the insertion of four Li atoms. Up to six Li, the band gap vanishes which indicates that the electronic conductivity of the SiOC molecule can be enhanced by the dopant Li.

Si−O, C−C, Si−C, Li−C, and Li−O atoms to be bonded if their distances are within 110% of their original bond length in bulk lattice which are determined by X-ray and neutron diffraction,[27−30] corresponding to the values of 1.85, 1.65, 2.09, 2.35, and 2.16 Å, respectively. Overall, the coordination numbers of Si−C and C−C remain nearly constant through the entire lithiation process. In the first stage of lithiation (Li composition below $Li_{42}Si_{28}O_{42}C_{68}$), the coordination number of Si−O decreases slowly showing that little change in chemical bonding is involved as Li gradually fills in the nanovoids. After saturation of the nanovoids (Li composition above $Li_{42}Si_{28}O_{42}C_{68}$), further Li insertion is accommodated by the breaking of Si−O bonds which results in the decrease of the coordination number of Si−O at a constant rate. Figure 3b shows that Li is mainly attracted by O and C atoms as seen in the monotonic increase of the coordination number of Li−O and Li−C. The interaction of Li with anionic O tends to break the Si−O bonds and forms new bonds of Li−O during lithiation. Furthermore, the unsaturated C atoms provide an additional site to accommodate Li insertion through geometry optimization and bond switching, with more details discussed in the following figure, instead of through the C−C or Si−C bond-breaking mechanism.

The statistical evolution of the SiOC tetrahedral units provides more information on the structural transformation of the amorphous network. We plot the evolution of the number of the tetrahedral units as a function of Li concentration in Figure 3c, in which the red line represents the variation of the Si−O−C units close to the segregated C network, and the blue line shows the number of tetrahedral units which are located inside the lattice and are caged by the C cellular network. It should be noted that there are no clear bounds between the two types of units. The statistics rather offers a qualitative understanding on the Li reaction pathway. The number of the tetrahedral units caged in the network follows the same steady decreasing trend of the coordination number of Si−O. On the contrary, the tetrahedral units residing nearby the C network remain almost unperturbed during lithiation. Li insertion mainly causes the structural rearrangement within the Si−O−C network, whereas the segregated C phase with the surrounding tetrahedral units is mostly preserved. The sp^2 graphene-like carbon network functions as the backbone to stabilize the entire molecule structure during lithiation. A similar finding was reported in a previous modeling of carbon-rich SiOC structures.[31] Figure 3d shows the comparison of the RDF of Si−O and C−C bonds in pristine and fully lithiated SiOC. For the Si−O bond, the peak of the RDF significantly decreases after lithiation, which originates from the Si−O bond breaking and dissociation of the tetrahedral units. The difference between the RDFs of C−C before and after lithiation is very small, thanks to the stable bonding of C−C.

In summary, the local bonding statistics reveals the following facts: (1) little change of chemical bonding is involved when Li fills in the nanovoids from the pristine SiOC. (2) When the nanovoids are saturated, Li insertion is accommodated by the Si−O bond breaking and unsaturated C atoms in the interior

DOI: 10.1021/acsami.7b10906
ACS Appl. Mater. Interfaces 2017, 9, 35001−35009

SiOC tetrahedral units as well as the topological defects at the edge of or within the carbon network. (3) The segregated sp^2 C interface remains inactive during lithiation and maintains the mechanical stability of the molecule structure.

We now focus on the second lithiation stage and examine the complex and concurrent microscopic events associated with Li reactions. Figure 4a shows four representative configurations in the course of lithiation, $Si_{28}O_{42}C_{68}$, $Li_{42}Si_{28}O_{42}C_{68}$, $Li_{70}Si_{28}O_{42}C_{68}$, and $Li_{104}Si_{28}O_{42}C_{68}$, respectively. It is clearly seen that the segregated C interface remains intact in the lithiation process. The overall structure retains the integrity with little change in shape and a volumetric expansion of 22% after full lithiation. Meanwhile, the Si−O−C tetrahedral units gradually vanish, thus decreasing the connectivity of the glass network and resulting in a possible open structure to accommodate further Li. Figure 4b shows the evolution of three local configurations representing the typical events in the respective configurations in Figure 4a. The Si−O bond is stretched and is eventually broken with more Li attracted by O. For the C phase, Li is attracted by the unsaturated C atoms of dangling bonds in the Si−O−C network as well as by the topological defects at the edge of or within the graphene-like segregated network. The absorption of Li by C is mediated by the geometric perturbation and bond switching. In Figure 4b, we show that the Si−C−C−Si clusters with unsaturated C atoms alter their geometry because of the electrostatic interactions induced by the surrounding Li. Specifically, the bond angles of Si−C−C−Si change from 99°, 161° to 126°, 129°, respectively, indicating that the centered unsaturated C optimizes toward the sp^2 type which has a planar symmetry of a characteristic angle of 120°. The MOs of the Si−C−C−Si cluster, to be discussed later, will provide a further understanding on the geometry changes. The third case in Figure 4b shows the Si−C bond breaking and the C−C bond reforming which result in the formation of the five-membered ring including one Si and four C atoms.

In fact, the sp^2 optimization of C through geometry relaxation is a common phenomenon facilitated by Li insertion. In pristine SiOC, many C atoms are unsaturated with one or more dangling bonds near the edge of the C network or in the Si−O−C network. We calculate the bond angle of C−C−C, Si−C−C, and Si−C−Si clusters in five different Li_xSiOC compositions. All clusters share the feature that the centered C atoms coordinated to the neighboring Si or C have one dangling bond compared with the stable sp^2 configuration. The evolution of the bond angle distributions in the five representative configurations is shown in Figure 5. Two characteristics of the bond angle distribution are that the bond angles larger than 145° steadily decrease, whereas the probability of bond angles between 115° and 130° significantly increases upon lithiation. This confirms the geometry optimization of C toward the sp^2-type configuration initiated by the imperfections of C atoms and coordinated by Li insertion. We may understand such a behavior from the hybridized MOs. At the ground state, a C atom containing six electrons has the electron configuration of $1s^22s^22p^2$. Two unpaired electrons occupy the outer shell, namely, p_y and p_z.[32,33] Figure 6 shows the evolution of two MOs mostly contributed by two centered C atoms. The blue and red isosurfaces correspond to the positive and negative values of the wave function. Before lithiation, the p_y orbital of two C atoms with the same orientation overlaps with each other to form one π-type MO,[34] π_y, as shown in Figure 6a. Similarly, two p_z orbitals overlap to form the π_z MO (Figure 6b). For C, one electron can be readily excited from 2s into the 2p state given a small energy difference between the two states.[35] In the presence of an external perturbation, such as a nearby hydrogen, the energy difference can be easily overcome and can result in the hybrid state of an sp orbital.[36] As shown in Figure 6c, the overlapped π_y is perturbed by the virtual orbital of nearby Li atoms (not shown in the MO diagram) and is split into two atomic orbitals of different orientations, which drives the formation of a hybrid sp^2 orbital. The sp^2 hybridization has the planar symmetry with a characteristic angle of 120° between each hybrid orbital of C atoms which is consistent with the result in the previous figure. This helps to understand the geometry changes of the C-centered Si−C clusters upon Li insertion. Figure 6b,d shows the π_z MO of C atoms before and after lithiation. There is no clear difference between the MO shapes for π_z in the two figures. It shows that the p_z orbital of C atoms is unperturbed by the surrounding Li and remains perpendicular to the sp^2 hybrid planar orbitals.

We further examine in detail the charge transfer from Li to the host Si−O−C molecule. We analyze the map of electron-density difference in various local regions. In Figure 7, from left to right, it shows the charge transfer in the segregated C interface, Si−O−C mixed regime, and amorphous silica domain before and after Li addition, respectively. The results are obtained by subtracting the charge density of pristine SiOC and pure Li from that of lithiated SiOC. All atomic positions are assumed to remain unchanged upon lithiation. In the graphene-like C network, charge transfer mainly takes place at the imperfection sites such as the five- or seven-membered C rings or at the edge of C atoms, which agrees with the previous experimental report.[14] Little chemical bonding of Li with the saturated sp^2-type C atoms is formed in the interior of the segregated C network. This again confirms the backbone function of the C interface and the resulting small deformation of the SiOC molecule in the lithiation process. In the mixed Si−O−C regime, the bonding environment is rather complicated. From the plot, we learn that the charge transfer mainly occurs around the O atoms and the unsaturated C atoms. In the SiO_4 tetrahedral units away from the C interface, a major fraction of the electron density is accumulated at the O atoms possibly because of the local screening effect of O.[37] The distribution map of the electron-density difference confirms that the major interaction occurs between Li with O and unsaturated C atoms in SiOC. These chemical interactions induce the breaking of Si−O bonds and the geometry perturbation of Si−C clusters.

The electron transfer also infers the electrical conductivity of the Si-based glass ceramics. One drawback of certain SiOC molecules is the electrically insulating nature which results in the poor charge transfer and voltage hysteresis in batteries. Doping and compositing with conductive agents are effective strategies to enhance the electrical conductivity of SiOC.[38−40] Here, we plot the electron density of states (DOS) of Li_xSiOC to show the remarkable improvement of electrical conductivity of SiOC induced by the Li dopant. Figure 8a−d shows the DOS of pristine SiOC, $Li_2Si_{28}O_{42}C_{68}$, $Li_4Si_{28}O_{42}C_{68}$, and $Li_6Si_{28}O_{42}C_{68}$, respectively. The Fermi energies have been shifted to zero on the energy scale. The DOS of pristine SiOC has a clear insulator character with a band gap of ca. 1.3 eV. However, the gap between the valence and conduction bands is much smaller compared with that of pure silica glass[22] because of the electron states around the Fermi level induced by the excess C in SiOC.[41] With the addition of Li, the electron states of Li are transferred to the low-energy unoccupied valence regimes brought by the chemical bonding of Li with unsaturated C atoms. The band gap is dramatically reduced by the insertion of four Li atoms. Up to six Li, $Li_6Si_{28}O_{42}C_{68}$ shows the conductor character without the

DOI: 10.1021/acsami.7b10906
ACS Appl. Mater. Interfaces 2017, 9, 35001−35009

band gap. This confirms that the electrical conductivity of SiOC can be largely enhanced by the doping elements such as Li and B[38,39] partially because of the presence of the excess C atoms.

CONCLUSIONS

We investigate the thermodynamics of Li reactions in a polymer-derived glass ceramic SiOC with a focus of understanding of the high capacity and structural stability of the host material upon lithiation. We build the carbon-rich SiOC molecule featuring the continuous Si−O−C tetrahedral units caged by the segregated C cellular network and nanovoids percolated in the lattice. The two-step lithiation proceeds by the absorption of Li at the nanovoid sites, followed by the chemical interactions of Li with the SiO_xC_{4-x} tetrahedral units and the C phase. The successive microscopic events are mediated by the Li anchoring at the nanovoids and the defect sites at the edge of or within the C network, bond breaking of Si−O, geometry perturbation of excess C atoms, and rearrangement of Si−C clusters. The structural stability stems from the backbone of the segregated C interface which remains intact during Li insertion. Furthermore, the amorphous network decreases its size in the first lithiation stage because of the local electrostatic interactions, whereas the geometry perturbation of unsaturated C atoms in the second lithiation step preserves Si−C and C−C bonds, both contributing to the mechanical stability of the molecule structure. We examine in detail the charge transfer in the local bonding environment to fully understand the Li chemistry with the constituents of the heterogeneous glassy lattice. The analysis of DOS supports the enhancement of the electrical conduction of SiOC by the doping elements.

AUTHOR INFORMATION

Corresponding Author

*E-mail: kjzhao@purdue.edu.

ORCID

Kejie Zhao: 0000-0001-5030-7412

Notes

The authors declare no competing financial interest.

ACKNOWLEDGMENTS

We acknowledge the support by the National Science Foundation through the grant CBET-1603866 and CMMI-1726392 and the support by the Office of Naval Research's NEPTUNE Program under the grant number N00014-16-1-3109. This project was initiated by a discussion with Prof. Gurpreet Singh at Kansas State University.

REFERENCES

(1) Kasavajjula, U.; Wang, C.; Appleby, A. J. Nano- and Bulk-silicon-based Insertion Anodes for Lithium-ion Secondary Cells. *J. Power Sources* **2007**, *163*, 1003−1039.

(2) Singh, V.; Joung, D.; Zhai, L.; Das, S.; Khondaker, S. I.; Seal, S. Graphene Based Materials: Past, Present and Future. *Prog. Mater. Sci.* **2011**, *56*, 1178−1271.

(3) Zhang, S.; Zhao, K.; Zhu, T.; Li, J. Electrochemomechanical Degradation of High-Capacity Battery Electrode Materials. *Prog. Mater. Sci.* **2017**, *89*, 479−521.

(4) Xu, R.; Zhao, K. Electrochemomechanics of Electrodes in Li-Ion Batteries: A Review. *J. Electrochem. Energy Convers. Storage* **2016**, *13*, 030803.

(5) Krishnan, R.; Lu, T.-M.; Koratkar, N. Functionally Strain-graded Nanoscoops for High Power Li-ion Battery Anodes. *Nano Lett.* **2011**, *11*, 377−384.

(6) Kim, H.; Cho, J. Superior Lithium Electroactive Mesoporous Si@carbon Core−shell Nanowires for Lithium Battery Anode Material. *Nano Lett.* **2008**, *8*, 3688−3691.

(7) Yao, Y.; McDowell, M. T.; Ryu, I.; Wu, H.; Liu, N.; Hu, L.; Nix, W. D.; Cui, Y. Interconnected Silicon Hollow Nanospheres for Lithium-ion Battery Anodes with Long Cycle Life. *Nano Lett.* **2011**, *11*, 2949−2954.

(8) Bhandavat, R.; Pei, Z.; Singh, G. Polymer-derived Ceramics as Anode Material for Rechargeable Li-ion Batteries: A Review. *Nanomater. Energy* **2012**, *1*, 324−337.

(9) David, L.; Bhandavat, R.; Barrera, U.; Singh, G. Silicon Oxycarbide Glass-graphene Composite Paper Electrode for Long-cycle Lithium-ion Batteries. *Nat. Commun.* **2016**, *7*, 10998.

(10) Ahn, D.; Raj, R. Thermodynamic Measurements Pertaining to the Hysteretic Intercalation of Lithium in Polymer-derived Silicon Oxycarbide. *J. Power Sources* **2010**, *195*, 3900−3906.

(11) Shen, J.; Ahn, D.; Raj, R. C-rate Performance of Silicon Oxycarbide Anodes for Li^+ Batteries Enhanced by Carbon Nanotubes. *J. Power Sources* **2011**, *196*, 2875−2878.

(12) Fukui, H.; Nakata, N.; Dokko, K.; Takemura, B.; Ohsuka, H.; Hino, T.; Kanamura, K. Lithiation and Delithiation of Silicon Oxycarbide Single Particles with A Unique Microstructure. *ACS Appl. Mater. Interfaces* **2011**, *3*, 2318−2322.

(13) Shen, J.; Raj, R. Silicon-oxycarbide Based Thin Film Anodes for Lithium Ion Batteries. *J. Power Sources* **2011**, *196*, 5945−5950.

(14) Fukui, H.; Ohsuka, H.; Hino, T.; Kanamura, K. A Si−O−C Composite Anode: High Capability and Proposed Mechanism of Lithium Storage Associated with Microstructural Characteristics. *ACS Appl. Mater. Interfaces* **2010**, *2*, 998−1008.

(15) Xu, R.; de Vasconcelos, L. S.; Zhao, K. Computational Analysis of Chemomechanical Behaviors of Composite Electrodes in Li-ion Batteries. *J. Mater. Res.* **2016**, *31*, 2715−2727.

(16) Oganov, A. R.; Glass, C. W. Crystal Structure Prediction Using ab Initio Evolutionary Techniques: Principles and Applications. *J. Chem. Phys.* **2006**, *124*, 244704.

(17) Renlund, G. M.; Prochazka, S.; Doremus, R. H. Silicon Oxycarbide Glasses: Part I. Preparation and Chemistry. *J. Mater. Res.* **1991**, *6*, 2716−2722.

(18) Ding, H.; Demkowicz, M. J. Hydrogen Reverses the Clustering Tendency of Carbon in Amorphous Silicon Oxycarbide. *Sci. Rep.* **2015**, *5*, 13051.

(19) Kresse, G.; Furthmüller, J. Efficient Iterative Schemes for ab Initio Total-energy Calculations Using a Plane-wave Basis Set. *Phys. Rev. B: Condens. Matter Mater. Phys.* **1996**, *54*, 11169.

(20) Kresse, G.; Joubert, D. From Ultrasoft Pseudopotentials to the Projector Augmented-Wave Method. *Phys. Rev. B: Condens. Matter Mater. Phys.* **1999**, *59*, 1758.

(21) Lee, D.; Vlassak, J. J.; Zhao, K. First-principles Theoretical Studies and Nanocalorimetry Experiments on Solid-state Alloying of Zr−B. *Nano Lett.* **2015**, *15*, 6553−6558.

(22) Zhang, Y.; Li, Y.; Wang, Z.; Zhao, K. Lithiation of SiO_2 in Li-ion Batteries: in situ Transmission Electron Microscopy Experiments and Theoretical Studies. *Nano Lett.* **2014**, *14*, 7161−7170.

(23) Frisch, M.; Trucks, G.; Schlegel, H.; Scuseria, G.; Robb, M.; Cheeseman, J.; Scalmani, G.; Barone, V.; Mennucci, B.; Petersson, G. *Gaussian 09 Package*; Gaussian Inc.: Wallingford, CT, USA, 2009.

(24) Lu, T.; Chen, F. Multiwfn: A Multifunctional Wavefunction Analyzer. *J. Comput. Chem.* **2012**, *33*, 580−592.

(25) Yu, L.; Raj, R. On the Thermodynamically Stable Amorphous Phase of Polymer-derived Silicon Oxycarbide. *Sci. Rep.* **2015**, *5*, 14550.

(26) Liao, N.; Zheng, B.; Zhou, H.; Xue, W. Lithiation Behavior of High Capacity SiCO Anode Material for Lithium-ion Battery: A First Principle Study. *Electrochim. Acta* **2015**, *156*, 115−120.

(27) Brequel, H.; Sorarù, G. D.; Schiffini, L.; Enzo, S. Radial Distribution Function of Amorphous Silicon Oxycarbide Compounds. *J. Metastable Nanocryst. Mater.* **2000**, *8*, 677−682.

(28) Bréquel, H.; Parmentier, J.; Walter, S.; Badheka, R.; Trimmel, G.; Masse, S.; Latournerie, J.; Dempsey, P.; Turquat, C.; Desmartin-Chomel, A. Systematic Structural Characterization of the High-

DOI: 10.1021/acsami.7b10906
ACS Appl. Mater. Interfaces 2017, 9, 35001−35009

temperature Behavior of Nearly Stoichiometric Silicon Oxycarbide Glasses. *Chem. Mater.* **2004**, *16*, 2585−2598.
(29) Schiemenz, B.; Power, P. P. Synthesis and Structure of a Unique Monomeric σ-Bonded Aryllithium Compound Stabilized by a Weak Li—Benzene π Interaction. *Angew. Chem., Int. Ed. Engl.* **1996**, *35*, 2150−2152.
(30) Chen, H.; Jutzi, P.; Leffers, W.; Olmstead, M. M.; Power, P. P. Synthesis and Structural Characterization of the Sandwichlike Compound [(12-crown-4)Li(η^5-C_5H_5)] and the η^0-Substituted-cyclopentadienide Salt [Li(12-crown-4)$_2$][1,2,4-$(Me_3Si)_3C_5H_2$]. *Organometallics* **1991**, *10*, 1282−1286.
(31) Liao, N.; Zheng, B.; Zhang, M.; Xue, W. Atomic Investigation on Reversible Lithium Storage in Amorphous Silicon Oxycarbide as a High Power Anode Material. *J. Mater. Chem. A* **2016**, *4*, 12328−12333.
(32) Bent, H. A. An Appraisal of Valence-bond Structures and Hybridization in Compounds of the First-row elements. *Chem. Rev.* **1961**, *61*, 275−311.
(33) Pierson, H. O. *Handbook of Carbon, Graphite, Diamonds and Fullerenes: Processing, Properties and Applications*; William Andrew: NJ, 2012.
(34) Albright, T. A.; Burdett, J. K.; Whangbo, M.-H. *Orbital Interactions in Chemistry*, 2nd ed.; John Wiley & Sons: Hoboken, NJ, 2013.
(35) Mathur, R. B.; Singh, B. P.; Pande, S. *Carbon Nanomaterials: Synthesis, Structure, Properties and Applications*; CRC Press: FL, 2016.
(36) Peschel, G. Carbon-carbon bonds: hybridization. http://www.physik.fu-berlin.de/einrichtungen/ag/ag-reich/lehre/Archiv/ss2011/docs/Gina_Peschel-Handout.pdf (accessed May 5, 2011).
(37) Sun, H.; Zhao, K. Electronic Structure and Comparative Properties of $LiNi_xMn_yCo_zO_2$ Cathode Materials. *J. Phys. Chem. C* **2017**, *121*, 6002−6010.
(38) Hermann, A. M.; Wang, Y.-T.; Ramakrishnan, P. A.; Balzar, D.; An, L.; Haluschka, C.; Riedel, R. Structure and Electronic Transport Properties of Si-(B)-C-N Ceramics. *J. Am. Ceram. Soc.* **2001**, *84*, 2260−2264.
(39) Riedel, R.; Bill, J.; Kienzle, A. Boron-modified Inorganic Polymers—Precursors for the Synthesis of Multicomponent Ceramics. *Appl. Organomet. Chem.* **1996**, *10*, 241−256.
(40) Tamayo, A.; Peña-Alonso, R.; Rubio, F.; Rubio, J.; Oteo, J. L. Synthesis and Characterization of Boron Silicon Oxycarbide Glass Fibers. *J. Non-Cryst. Solids* **2012**, *358*, 155−162.
(41) Kroll, P. Tracing Reversible and Irreversible Li Insertion in SiCO Ceramics with Modeling and ab-initio Simulations. *MRS Online Proc. Libr.* **2011**, *1313*, 1−6.

DOI: 10.1021/acsami.7b10906
ACS Appl. Mater. Interfaces 2017, 9, 35001−35009